Published in final edited form as:

Neuroimage. 2020 October 15; 220: 117111. doi:10.1016/j.neuroimage.2020.117111.

Single-scale time-dependent window-sizes in sliding-window dynamic functional connectivity analysis: A validation study

Xiaowei Zhuang[a,1], **Zhengshi Yang**[a,1], **Virendra Mishra**[a], **Karthik Sreenivasan**[a], **Charles Bernick**[a,b], **Dietmar Cordes**[a,c,d,*]

[a]Cleveland Clinic Lou Ruvo Center for Brain Health, Las Vegas, NV, USA

[b]UW Medicine, Seattle, WA, USA

[c]University of Colorado, Boulder, CO, USA

[d]Department of Brain Health, University of Nevada, Las Vegas, NV, USA

Abstract

During the past ten years, dynamic functional connectivity (FC) has been extensively studied using the sliding-window method. A fixed window-size is usually selected heuristically, since no consensus exists yet on choice of the optimal window-size. Furthermore, without a known ground-truth, the validity of the computed dynamic FC remains unclear and questionable. In this study, we computed single-scale time-dependent (SSTD) window-sizes for the sliding-window method. SSTD window-sizes were based on the frequency content at every time point of a time series and were computed without any prior information. Therefore, they were time-dependent and data-driven. Using simulated sinusoidal time series with frequency shifts, we demonstrated that SSTD window-sizes captured the time-dependent period (inverse of frequency) information at every time point. We further validated the dynamic FC values computed with SSTD window-sizes with both a classification analysis using fMRI data with a low sampling rate and a regression analysis using fMRI data with a high sampling rate. Specifically, we achieved both a higher classification accuracy in predicting cognitive impairment status in fighters and a larger explained behavioral variance in healthy young adults when using dynamic FC matrices computed with SSTD window-sizes as features, as compared to using dynamic FC matrices computed with the conventional fixed window-sizes. Overall, our study computed and validated SSTD window-sizes in the sliding-window method for dynamic FC analysis. Our results demonstrate that dynamic FC matrices computed with SSTD window-sizes can capture more temporal dynamic information related to behavior and cognitive function.

*Corresponding author. Cleveland Clinic Lou Ruvo Center for Brain Health., 888 W. Bonneville Ave, Las Vegas, NV, 89106, USA. cordesd@ccf.org (D. Cordes).

[1]These authors contributed equally to this manuscript.

CRediT authorship contribution statement

Xiaowei Zhuang: Conceptualization, Methodology, Validation, Writing - original draft, Software. **Zhengshi Yang:** Conceptualization, Methodology, Validation, Writing - original draft, Software. **Virendra Mishra:** Resources. **Karthik Sreenivasan:** Resources. **Charles Bernick:** Resources. **Dietmar Cordes:** Supervision, Conceptualization, Methodology, Writing - review & editing.

Appendix A. Supplementary data

Supplementary data to this article can be found online at https://doi.org/10.1016/j.neuroimage.2020.117111.

Keywords

Dynamic functional connectivity (FC); Single-scale time-dependent (SSTD) window-sizes; Sliding-window analysis; Regression and classification analysis; Empirical mode decomposition (EMD)

1. Introduction

Brain functional connectivity (FC) has been widely studied using resting-state functional magnetic resonance imaging (fMRI), and is most commonly assessed using Pearson's correlation coefficient among distributed brain regions (Biswal et al., 1995). Many studies have identified a set of statistically interdependent regions where the blood-oxygenated-level-dependent (BOLD) signals are temporally correlated in the absence of an explicit task (Biswal et al., 2010; De Luca et al., 2005; Greicius, 2008; Greicius et al., 2003). Investigating resting-state FC has provided fundamental insight into basic neural function and disease conditions (Bai et al., 2009; Damoiseaux et al., 2006; Fox et al., 2005; Greicius et al., 2004; Smith et al., 2009).

More recently, studies have demonstrated that instead of being temporally static, FC can change periodically over time during an fMRI scan (Allen et al., 2014; Chang and Glover, 2010; Jones et al., 2012; Liu and Duyn, 2013; Majeed et al., 2011; Sakoğlu et al., 2010; Smith et al., 2012). Dynamic FC analysis has been proposed to investigate and understand these periodic temporal changes (see Calhoun et al., 2014; Hutchison et al., 2013; Preti et al., 2017 for reviews). Altered dynamic FC have been reported in various neurological disorders such as schizophrenia (Damaraju et al., 2014), Alzheimer's disease (Jones et al., 2012), Parkinson's disease (Cordes et al., 2018), major depression disorders (Holtzheimer and Mayberg, 2011), and autism (Price et al., 2014). All of these findings demonstrate the pathophysiologic relevance of dynamic FC across multiple diseased populations, and thus investigating dynamic FC will lead to better understanding of these conditions.

Many methods have been proposed for dynamic FC analysis, such as the sliding-window method (Allen et al., 2014; Chang and Glover, 2010), multivariate volatility models (Lindquist et al., 2014), temporal independent component analysis (ICA) (Calhoun et al., 2001; Smith et al., 2012), the quasi-periodic pattern method (Majeed et al., 2011; Thompson et al., 2014), the hidden Markov model (Eavani et al., 2013), and co-activation pattern (CAP) analysis (Liu and Duyn, 2013). The sliding-window method captures the FC in a certain time window by calculating pairwise correlation or covariance, then shifts to the next time window and repeats the same procedure until the last fMRI volume. Dynamic FC is then characterized by the windowed covariance or correlation matrices. Multivariate volatility models, such as exponentially weighted moving average and dynamic conditional correlation methods, are parametric models of the conditional correlation between time courses which refine the concept of sliding-window. Temporal ICA decomposes each subject's fMRI time series into temporally independent components, defined as distinct functional modes. The quasi-periodic pattern method evaluates the spatiotemporal dynamics of the BOLD signals to identify a common whole-brain pattern that occurs periodically during an fMRI scan. The Hidden Markov model decodes connectivity dynamics into a

temporal sequence of hidden network “states” for each subject. The CAP analysis examines the dynamics of a specific resting-state network and tracks the variations of FC within each individual time frame.

Among all these methods, the sliding-window method is one of the most widely applied techniques in dynamic FC analysis due to its relative simplicity, and it has been successfully applied to reveal macro-scale spatiotemporal fluctuation of the brain in multiple diseased populations (Damaraju et al., 2014; Gonzalez-Castillo et al., 2015; Kiviniemi et al., 2011; Leonardi and Van De Ville, 2015; Yaesoubi et al., 2017; Yu et al., 2015). However, a few concerns remain unaddressed.

The first concern is the choice of window-size. Currently, there is no consensus on the optimum length of the window used in this method. Ideally, the window-size should be both small enough to capture temporal transients and large enough to produce stable and statistically powerful results (Hutchison et al., 2013). Leonardi and Van De Ville (2015) recommend choosing a window-size that exceeds the longest wavelength in the BOLD signal to avoid spurious connectivity fluctuations (~100s), which is termed the rule-of-thumb in window-size selection. Zalesky and Breakspear (2015) later validate this rule-of-thumb choice but also demonstrate that, theoretically, the dynamic FC can be stably detected with a much shorter window (~40s). The fundamental nature of choices for these fixed window lengths limits the dynamic FC analysis to the fluctuations in the frequency range below the window period, irrespective of the true frequency content of the data (Preti et al., 2017). In this case, a time-dependent window-size, based on the true frequency content of the fMRI time series, could more accurately capture the time-varying FC changes in the data and is necessary to the sliding-window method. Furthermore, adaptive window-sizes have already been successfully applied in other fields, including frequent item sets mining in data stream (Deypir et al., 2012; Li and Wang, 2017) and estimation of data center source utilization (Baig et al., 2020).

Another concern is how to validate the observed dynamic FC as true temporal variations instead of confounding noises. Multiple null models have been proposed to test the statistical significance of the dynamic FC variations (Hindriks et al., 2016; Zalesky et al., 2014). However, heterogeneous test results could be obtained from choosing different methods to produce surrogates and applying different test-statistics (Zalesky and Breakspear, 2015). Without a known ground truth, this procedure is data dependent and time-consuming. In this case, indirect validation from investigating the useful information carried by dynamic FC could be more appropriate to determine the significance of dynamic FC analysis. Previous studies have utilized dynamic FC information as features in classifying normal subjects from diseased populations (Rashid et al., 2016; Shen et al., 2010) and predict cognitive function at the individual level (Liégeois et al., 2019; Liu et al., 2018). Therefore, a reliable classification result with dynamic FC matrices as features suggests dynamic FC matrices capture true temporal variations that carry disease-relevant information. Furthermore, multiple studies have revealed associations between static FC matrices and behavioral assessments such as age (Allen et al., 2011), gender (Zhang et al., 2018), intelligence (Song et al., 2008), cognition and emotions (Greicius et al., 2003), which demonstrate the behavioral and clinical relevance of static FC matrices. However, the associations between

dynamic FC matrices computed from the sliding-window method and behavioral assessments have not been investigated yet and remain a potential tool for validating the observed dynamic FC as a true temporal variation that carries behavioral-relevant information.

Taken together, in this study, we first computed single-scale time-dependent (SSTD) window-sizes at every time point in the sliding-window approach using empirical mode decomposition (EMD). With SSTD window-sizes we refer to exactly *one* window-size per time point instead of multiple window-sizes per time point (as in *multi-scale* window-sizes). EMD is a data-adaptive analysis method for studying the naturally occurring frequency bands in time series, which can be used for non-stationary signals and allows the decomposition of time series into nearly orthogonal modes spanning narrow frequency bands (Huang, 2005). Decomposed signals from EMD track local periodic changes of non-stationary time series and time-dependent window-sizes can be determined at each time point. Multi-scale time-dependent window-sizes based on EMD were first proposed in Chen et al. (2010), where multiple window-sizes were computed for a single time point. Multi-scale time--dependent window-sizes have been successfully applied in dynamic analysis of temperature changes and dissolved oxygen time series (Huang and Schmitt, 2014). However, correlation values computed from multiple window-sizes at a single time point between two time series are difficult to interpret in terms of dynamic FC. In this case, our group first used a weighted average to combine these multi-scale window-sizes in Cordes et al. (2018). In this study, we further improved this method to produce more stable results and termed it SSTD window-sizes. We also demonstrated the reliability of SSTD window-sizes in capturing frequency information at every time-point using simulated time series.

We next computed the standard deviation matrices over all slided windows with SSTD window-sizes to quantify the dynamic FC. We validated dynamic FC matrices computed from SSTD window-sizes with both a regression analysis using *Human Connectome Project* (HCP) (Van Essen et al., 2013) data with a high sampling rate and a classification framework using *Professional Fighters Brain Health Study* (PFBHS) (Bernick et al., 2013) data with a conventional sampling rate. Dynamic FC matrices computed with SSTD window-sizes were compared with those computed with conventional fixed window-sizes in both analyses.

2. Methods

2.1. Computation of SSTD window-sizes

2.1.1. EMD decomposition—EMD uses a sifting algorithm to decompose the original multicomponent time series into nearly orthogonal modes spanning narrow frequency bands (Patrick and Goncalves, 2004), which are named intrinsic mode functions (IMFs). Let $y(t) \in \mathbb{R}^{N \times 1}$ denote the resting-state time series from a single voxel and N is the total number of time points. To avoid unstable EMD decomposition results at the starting and ending point of $y(t)$, a new time series $\tilde{y}(t)$ is first created by:

$$\tilde{y}(t) = [\text{flip}(y(t)), \quad y(t), \text{flip}(y(t))], \tag{1}$$

where flip($y(t)$) reverses the order of the time points in $y(t)$. $\tilde{y}(t)$ is then intensity normalized and decomposed into K IMFs using the sifting algorithm (Patrick and Goncalves, 2004):

$$\tilde{y}(t) = \sum_{i=1}^{K} c_i(t) + r_K(t), \tag{2}$$

where $c_i(t)$ is the ith IMF and $r_K(t)$ is the residual function. The number of IMFs (K) here is determined from the data itself during the sifting algorithm. IMFs obtained from EMD are naturally oscillating functions and with frequency contents in a descending order, i.e. $c_1(t)$ contains the highest frequency component and $c_K(t)$ contains the lowest. The residual $r_K(t)$ contains only the trend-level frequency component.

2.1.2. Instantaneous period and average energy—The instantaneous period is computed only for the center part of each IMF $c_i(t)$, which corresponds to the time points in the original signal. For each IMF, the instantaneous frequency $f_i(t)$ is first computed using the Hilbert Transform by extending $c_i(t)$ into the complex domain (Huang, 2005; Huang and Shen, 2014; Huang and Wu, 2008). The instantaneous period $p_i(t)$ is then defined as $\frac{1}{f_i(t)}$. Furthermore, since $\tilde{y}(t)$ has been intensity normalized, the energy of each IMF is defined as $E_i = \frac{1}{T}\sum_{t=1}^{T} c_i(t)^2$. In this case, the instantaneous periods $p_i(t)$ capture the local non-stationarity of the original signal, and the average energy densities E_i summarize the energy contributions of each IMF to the original signal.

2.1.3. SSTD window-sizes of two fMRI time series $y^{(1)}(t)$ and $y^{(2)}(t)$—Following the above steps, we have computed $p_i^{(1)}(t)$ and $p_i^{(2)}(t)$ to denote the instantaneous period at time t for IMFs $c_i^{(1)}(t)$ corresponding to $y^{(1)}(t)$ and $c_i^{(2)}(t)$ corresponding to $y^{(2)}(t)$, respectively. We also have computed $E_i^{(1)}$ and $E_i^{(2)}$ for the average energy corresponding to each $c_i^{(1)}(t)$ and $c_i^{(2)}(t)$. We then define a weighted instantaneous period for each $y^{(m)}(t)$, ($m = 1, 2$) as

$$P_{y^{(m)}}(t) = \frac{1}{\left(\sum_{i=1}^{K} E_i^{(m)}\right)} \sum_{i=1}^{K} p_i^{(m)}(t) \times E_i^{(m)}, \quad m = 1, 2. \tag{3}$$

SSTD window-size of $y^{(1)}(t)$ and $y^{(2)}(t)$ is finally defined as:

$$P_f\left(t; y^{(1)}, y^{(2)}\right) = \max\left(P_{y^{(1)}}(t), P_{y^{(2)}}(t)\right). \tag{4}$$

Furthermore, for noisy time series with limited durations, IMFs with low frequencies may not be sufficiently covered by the length of time series, and EMD may lead to non-orthogonal components at very low frequencies. These IMFs usually contain longer instantaneous period but lower energy. Therefore, in computing the weighted instantaneous

period for each $y^{(m)}(t)$, (m = 1, 2) using Eq. (3), IMFs with energy less than of the total energy have been excluded.

2.2. Validation with simulation

We demonstrate through simulation that SSTD window-sizes can represent the true period (frequency) information at every time point. To this end, we considered two pure sinusoidal signals. The first signal was a cosine wave with frequency f_1 suddenly switching to f_2 at a certain time point:

$$y^{(1)} = \begin{cases} \cos(2\pi f_1 t), & t = \left(1 : \frac{2N}{3}\right) \times TR \\ \cos(2\pi f_2 t), & t = \left(\frac{2N}{3} + 1 : N\right) \times TR \end{cases},$$

where TR was the repetition time (inverse of the sampling rate) and N was the total number of time points. The other signal was a simple cosine wave with a fixed frequency f_3:

$$y^{(2)} = \cos(2\pi f_3 t), \quad t = (1 : N) \times TR.$$

In our simulation, we chose f_1 = 0.02 Hz, f_2 = 0.05 Hz and f_3 = 0.04 Hz, respectively. The total duration of time series was set to 300s (5mins), and the frequency shift of $y^{(1)}$ happened at t = 200s. We chose the TR to be 0.72s and 2.8s, respectively, to mimic the two real fMRI data used in this study (described in more details in section 2.3 and 2.4). N was set to be $\frac{300s}{TR}$ in each case. SSTD window-sizes were determined as described in section 2.1. Dynamic FC values between $y^{(1)}$ and $y^{(2)}$ were computed using the sliding-window approach with SSTD window-sizes and fixed window-sizes of 30s, 60s and 100s.

2.3. Validation with classification analysis using fMRI data with low sampling rate

2.3.1. Subjects—65 cognitively non-impaired fighters and 68 cognitively impaired fighters from the *PFBHS* (Bernick et al., 2013) were included in our study. Their cognitive impairment status was predefined based on fighters' performance of the Finger Tapping test and Symbol Digit Coding test from the CNS Vital Signs tests (Gualtieri and Johnson, 2006). Cognitively non-impaired and impaired fighters were matched for age, gender, years of education, and fighting exposures (number of fights, years of fighting and knock-out counts). Detailed demographics are listed in Table 1(A).

MRI data were collected for all subjects on a 3T Siemens Verio scanner with a 32-channel head coil. Resting-state fMRI data were collected with following parameters: TR = 2.8s, TE = 28 ms, in-plane resolution 2mm × 2mm, slice thickness 4 mm, 30 axial slices and 137 time frames (6mins and 24s). In addition, a high resolution T1-weighted structural image was acquired using a standard 3D MPRAGE sequence.

2.3.2. Preprocessing—Each T1-weighted image was input into the FreeSurfer 6.0 processing pipeline (Fischl, 2012) to generate a subject-specific cortical and subcortical parcellation. 66 cortical labels from Desikan-Killiany atlas (Desikan et al., 2006), and 12

sub-cortical labels were defined as regions of interest (ROIs). This anatomical labeling was wrapped to each subject's fMRI space using a 12-parameters affine transform in Advanced Normalization Tools (ANTs) software (http://stnava.github.io/ANTs/).

The first 4 time frames (~12s) of fMRI data were removed to allow the MR signal to achieve T1 equilibrium. Remaining time frames were slice-timing corrected and realigned to the mean echo-planar image in SPM12 (http://www.fil.ion.ucl.ac.uk/spm/). FMRI data were further spatially smoothed using a 6 mm 3D-Gaussian filter in the subject fMRI space and high-pass filtered with a cosine filter with a cut-off frequency of 0.008 Hz. Nuisance regression was performed to further denoise the fMRI data, using six head motion parameters and CompCor generated white-matter (WM) and cerebrospinal fluid (CSF) signals (Behzadi et al., 2007). Finally, all voxel time courses were variance normalized.

2.3.3. Dynamic FC estimation—Average time series of each ROI were obtained in the subject's fMRI space. Static FC were estimated by computing the Pearson's correlation coefficient between time series from each ROI pair. Dynamic FC were estimated using the sliding-window method with both SSTD window-sizes and multiple conventional fixed window-sizes. Pearson's correlation between time series from all ROI pairs were computed within the defined window and the window was slided over 1 TR (2.8s). The standard deviation of Pearson's correlations over all windows were defined as the dynamic FC values for all pairs of ROIs and formed the dynamic FC matrices. This dynamic FC matrices then were used to represent whole-brain temporal dynamics.

2.3.4. Classification framework—Both static and dynamic FC were used as features to classify cognitive impairment status of fighters. Classification framework included an automated feature selection step and a radial basis functional classifier step (see Mishra et al., 2017, for details). A ten-fold cross-validation was used to determine the classification accuracy. The classification process was repeated 100 times to rule out the potential division bias in the ten-fold division. Classification accuracy, sensitivity (correctly classified impaired fighters), specificity (correctly classified nonimpaired fighters), and the area under the receiver operating characteristic curve (ROC) for all 100 iterations were used to evaluate the classifier performance.

2.4. Validation with regression analysis using fMRI data with a high sampling rate

2.4.1. Subjects—The same subjects used in our previous study (Yang et al., 2019) were used in this study. Briefly, 88 male subjects from *HCP* 1200 Subject Release (Van Essen et al., 2013; WU - Minn Consortium Human Connectome Project, 2017), who were 26 to 30 years old and completed both resting-state fMRI and T1-weighted structural scans, were included. Detailed demographic information is listed in Table 1 (B).

Resting-state fMRI data were acquired on 3T Siemens scanners using a Gradient-echo EPI sequence with the following parameters: multiband factor = 8, TR = 0.72s, TE = 33.1 ms, 2.0 mm isotropic voxels, 72 axial slices and 1200 time points (14mins and 24s). A high resolution T1-weighted structural image was acquired using a 3D MPRAGE sequence.

2.4.2. Behavioral measurements—56 behavioral measurements were used to evaluate if the dynamic FC matrices computed with the proposed optimum window-size can better explain the behavioral variance than the dynamic FC matrices estimated with conventional fixed window-sizes. Initially, 64 behavioral measurements covering cognitive, social, emotion, personality traits, tobacco consumption, drug consumption, rule breaking, antisocial behavior, pain intensity, and externalization were included. Out of these 64 behavioral measurements, 8 were excluded from our analysis based on the following two criteria: 1) more than 5% of subjects did not have valid measurements; 2) the maximal value was more than 100 times the mean value, which suggested extreme outliers. Details of these 56 behavioral variables are listed in Supplementary Table S1.

2.4.3. Preprocessing—The minimally preprocessed resting-state fMRI data (in the standard MNI space) were downloaded from the HCP website (https://www.humanconnectome.org/study/hcp-young-adult/document/1200-subjects-data-release) and were treated as the raw fMRI data in our analysis. A more detailed description of HCP minimal preprocessing steps can be found in Glasser et al. (2013). Additionally, the first 15 vol (~11s) of fMRI data were discarded to avoid data with an unsaturated T1 signal, and the same nuisance regressors as used for the *PFBHS* data were used to further denoise the *HCP* data.

2.4.4. Dynamic FC estimation—Average time series from 112 regions of the automated anatomical labeling atlas (Tzourio-Mazoyer et al., 2002) were obtained. Static and dynamic FC matrices were estimated the same way as for the *PFBHS* data. Specifically, both SSTD window-sizes and multiple conventional fixed windows were used in the sliding-window approach. The window was slided over 4 time points (2.88s) due to the fast sampling rate.

2.4.5. Regression analysis—Static and dynamic FC matrices were rearranged as a single vector for each subject, and these vectors for all subjects were arranged in a matrix. Principal component analysis (PCA) was applied on the matrix to reduce data dimension and only those components that explain more than 1% of the variance were retained. Linear regression was applied for each behavioral measurement separately with PCA components as independent variables and the behavioral measure as the dependent variable. The coefficient of determination, namely R-squared, was used to measure the proportion of behavioral variance explained by the FC matrix (Draper and Smith, 1998). Subjects' age and handedness were used as covariates and regressed out from behavioral measurements prior to PCA.

3. Results

3.1. Validation with simulation

Simulated signals with TR = 0.72s and 2.8s give similar results, and therefore we include simulation results with TR = 0.72s here in Fig. 1. The simulation results with TR = 2.8s is included in supplementary Fig. S1. Simulated signals $y^{(1)}$ and $y^{(2)}$ are plotted in Fig. 1 (A). Corresponding frequency spectrums are shown in Fig. 1 (B). For time points before t = 200s,

$y^{(1)}$ is dominated by frequency f_1 = 0.02 Hz and $y^{(2)}$ is dominated by frequency f_3 = 0.04 Hz, and therefore the corresponding periods of $y^{(1)}$ is 50s (~70 TR) and of $y^{(2)}$ is 25s (~35 TR) in this time segment. For time points after t = 200s, $y^{(1)}$ is dominated by frequency f_2 = 0.05 Hz and $y^{(2)}$ is dominated by frequency f_3 = 0.04 Hz, and therefore the corresponding periods of $y^{(1)}$ is 20s (~28 TR) and of $y^{(2)}$ is 25s (~35 TR) in this time segment. As shown by the solid blue ($y^{(1)}$) and red lines ($y^{(2)}$) in Fig. 1 (D), the instantaneous periods computed from our method capture exactly these periods at almost all time points for both signals. The SSTD window-sizes are then set to be the larger period of the two signals, as shown by the dashed green lines in Fig. 1 (D). Multiple fixed window-sizes are also shown as dashed yellow, purple and light blue lines in Fig. 1 (D) for references. Fig. 1 (C) plots dynamic FC values computed from the sliding-window approach with SSTD window-sizes (solid green line) and multiple fixed window-sizes (dashed yellow, purple and light blue lines). As shown by the solid green line, using SSTD window-sizes in the sliding-window approach captures both the stable and small correlation between two signals at time points before t = 200s, and large variations of correlations between two signals at time points after t = 200s.

3.2. Validation with classification analysis

3.2.1. Average SSTD window-sizes—Average SSTD window-sizes computed from our method are 34.66s±2.29s for cognitively nonimpaired fighters and 34.20s± 2.29s for cognitively impaired fighters (Table 2). Histograms of average SSTD window-sizes for each subject are also shown in Fig. S2 (B). Thus, the main fixed window-size for comparison is chosen to be 35s (~12 TR). We further compute the dynamic FC matrices with fixed window-sizes of 60s (~21 TR) and 90s (~32 TR) as suggested in Hutchison et al. (2013) for comprehensive comparisons.

3.2.2. Classification results—Fig. 2 shows the classifier performance of the *PFBHS* data, with static FC (sFC, red), static and dynamic FC with fixed window-size of 35s (sFC&dFC-35s, green), and static and dynamic FC with SSTD window-sized (sFC&dFC-SSTD, purple) as features, respectively. Boxplots of the area under the ROC curve (A), accuracy (B), sensitivity (C), and specificity (D) are shown for 100 iterations. As shown in Fig. 2, adding temporal dynamics information significantly improves the classifier performance, as compared to using static FC information alone (green and purple boxes vs. red box). Using dynamic FC matrices computed with SSTD window-sizes further significantly improves the classifier performance, as compared to using dynamic FC matrices computed from the comparable fixed window-size ($p = 1.52 \times 10^{-10}$, purple box vs. green box).

Fig. 3 further plots areas under the ROC curves for classifications using static FC and dynamic FC with 35s (sFC&dFC-35s), 60s (sFC&dFC-60s), 90s (sFC&dFC-90s), and SSTD windows (sFC&dFC-SSTD) as features separately. Table 3 lists p-values of statistical comparisons (two-sample t-test) between classification results using different features. As shown in Fig. 3 and Table 3, using sFC&dFC-SSTD as features significantly outperforms sFC&dFC-35s ($p = 1.52 \times 10^{-10}$), sFC&dFC-60s ($p = 1.33 \times 10^{-11}$), and sFC&dFC-90s ($p = 3.04 \times 10^{-12}$) in classifying cognitive impairment status in fighters.

3.3. Validation with regression analysis

As listed in Table 2, the average SSTD window-sizes computed from the proposed method for *HCP* data is 32.73 ± 3.52s. Histograms of average SSTD window-sizes for each subject are also shown in Fig. S2 (A). In this case, the main fixed window-size for comparison is chosen to be 32.4s (~45 TR). Furthermore, since *HCP* data are acquired with a fast sampling rate, we can use a smaller window-size but still keep enough time points to compute the windowed FC matrix. Therefore, the dynamic FC matrices computed using the sliding-window approach with fixed window-sizes of 21s (~30 TR) and 65s (~90 TR) are further used for comprehensive comparisons.

Fig. 4 (A) plots the explained behavioral variance of *HCP* data using sFC, sFC&dFC-32s, and sFC&dFC-SSTD as features. As shown in Fig. 4 (A), significant larger variance is explained by both static and dynamic FC matrices than by static FC matrices alone (green and purple boxes vs. red box). Using dynamic FC matrices computed with SSTD window-sizes further increases the explained behavioral variance by 19.7% (purple box vs. green box) on average. Fig. 4 (B) further compares the performance of SSTD window-sizes with multiple fixed window-sizes in the regression analysis. As shown by the purple box, larger behavioral variances can be explained more by the dynamic FC matrices computed with SSTD window-sizes than by multiple fixed window-sizes (green boxes). Statistical significance levels (two-sample *t*-test) are listed in Table 4.

4. Discussion

In this study, we computed SSTD window-sizes in the sliding-window method for dynamic FC analysis. SSTD window-sizes of two time series were based on their frequency contents and were computed from the instantaneous period and average energy of each IMF obtained from the EMD method. Using simulated time series, we first demonstrated that SSTD window-sizes can capture the time-dependent frequency information in the time series. The optimum performances of dynamic FC matrices computed with SSTD window-sizes were further validated through both a classification analysis using the *PFBHS* data with a low sampling rate and a regression analysis using the *HCP* data with a high sampling rate. Specifically, both a higher classification accuracy in predicting cognitive impairment status in fighters and a larger explained behavioral variance in healthy young adults were achieved using dynamic FC matrices computed with SSTD window-sizes as features, as compared to using dynamic FC matrices computed with several conventional fixed window-sizes.

4.1. SSTD window-sizes are data-driven, time-dependent, and can capture the frequency content in simulated time series

SSTD window-sizes are based on the frequency content of the time series itself, and thus are purely data-driven. The frequency content of the time series is represented by the instantaneous period at every time point and therefore SSTD window-sizes are time-dependent. Simulated time series with known frequency contents are used to demonstrate that time-dependent and data-driven window-sizes can accurately capture the frequency information of the time series.

The simulated time-series are basic oscillatory and stationary functions with local means equal to zero, therefore the Hilbert Transform is well defined and produces meaningful non-negative instantaneous frequencies for these two time series (Huang and Shen, 2014). As shown in Fig. 1 (A), in our simulation, a sudden frequency switch from $f_1 = 0.02$ Hz to $f_2 = 0.05$ Hz happens at $t = 200$s for signal $y^{(1)}$ (Fig. 1 (A)), and the frequency for signal $y^{(2)}$ stays at $f_3 = 0.025$ Hz for the entire time series. The lowest frequency contained in simulated signals is therefore 0.02 Hz. According to the rule-of-thumb criteria (Leonardi and Van De Ville, 2015), the window-size used in the sliding-window approach should be larger than $\frac{1}{0.02} = 50$ s. However, dynamic FC values computed with choices following this rule miss the large periodic temporal variations after $t = 200$s and lead to a larger transition period (dashed light blue and purple lines in Fig. 1 (C)). Furthermore, dynamic FC values computed with a relatively small window are able to capture the large temporal variations after $t = 200$s, but create unstable and unreal large temporal variations before $t = 200$s (dashed yellow line in Fig. 1(C)). In some cases, dynamic FC values computed with a small window-size may even pass the statistical significance test, but the strong variability is still not real and is mainly the reason for the lack of degree of freedom in the calculation (Chen et al., 2010).

SSTD window-sizes, however, automatically capture the frequency switch in our simulation by outputting a window-size of 50s before $t = 200$s and another window-size of 25s after $t = 200$s (dashed green line in Fig. 1 (D)). This result demonstrates that SSTD window-sizes are time-dependent and capture the exact frequency information of the time-series. Furthermore, no prior information is required to calculate SSTD window-sizes and thus the procedure is purely data-driven. Dynamic FC values computed from SSTD window-sizes also give optimum performance, as they not only capture both large temporal variations in functional correlation between $y^{(1)}$ and $y^{(2)}$ after $t = 200$s but also correctly identify small correlation between $y^{(1)}$ and $y^{(2)}$ before $t = 200$s (solid green line in Fig. 1 (C)).

The simulation with TR = 2.8s (Fig. S1) gives similar results as the simulation with TR = 0.72s (Fig. 1), but the less time points of TR = 2.8s results in less smoothed curves in Fig. S1. Overall, as shown in Fig. 1 and Fig. S1, our simulation results demonstrate that SSTD window-sizes can capture frequency changes in time series.

4.2. SSTD window-sizes capture more meaningful temporal dynamics information of fMRI time series

Functional MRI time series are usually non-stationary. Therefore, in our method, we first decompose the original time series into multiple IMFs, which represent different scales of the original time series and form the adaptive and oscillating basis of the data (Chen et al., 2010; Huang, 2005; Huang et al., 1998). An IMF is defined as a basic oscillatory function with an extreme value followed by a zero-crossing (Patrick and Goncalves, 2004). Thus, the Hilbert Transform is well defined for an IMF (Huang and Shen, 2014). Furthermore, since the fMRI time series is first intensity normalized in our study and EMD is essentially a sifting algorithm that estimates an IMF and subtracts it successively (Eq. (2)), the average energy of each IMF represents weight and contribution of each IMF to the original signal in terms of intensity. Therefore, at each time point, we then use the average of instantaneous periods of all IMFs weighted by the corresponding energy (Eq. (3)) to represent the period

information of the original fMRI time series. We further demonstrate that the dynamic FC matrices computed using this energy-weighted period measurement can capture more cognitively and behaviorally meaningful information.

4.2.1. Both static and dynamic FC matrices contain disease and cognitive relevant information—Previous studies have demonstrated that FC matrices, both static and dynamic, can be used as feature sets to classify normal subjects from subjects with a cognitive disorder or disease. For example, using static FC matrices alone, Shen et al. (2010) achieved an accuracy of 92.3% in classifying schizophrenia patients from normal subjects. However, the small sample size (~50 in total) in Shen et al. (2010) limited its generalization. Rashid et al. (2016) used a much larger sample size (273) and demonstrated that using both static and dynamic FC as features, an accuracy level of 89% was achieved in classifying schizophrenia patients, bipolar patients, and normal subjects, which was significantly higher than using static FC matrices as features alone (59%). These studies have demonstrated that both static and dynamic FC contain disorder-related information. Furthermore, using static FC derived measurements, multiple studies have shown that high accuracy can be achieved in classifying normal subjects, subjects with mild cognitive impairment (MCI), and subjects with Alzheimer's disease (Challis et al., 2015; Chen et al., 2016; Khazaee et al., 2017; Wang et al., 2018). These studies further suggest that FC matrices contain cognitively meaningful information, as MCI and AD patients usually show significant loss in cognition (see Jack et al., 2013, for a review).

4.2.2. Both static and dynamic FC matrices contain behavioral meaningful information—Disease is not the only factor driving the structure involved in strength and flexibility of brain FC. Multiple studies have demonstrated that a battery of personal behaviors are encoded in functional brain connections as well, including intelligence (Liu et al., 2018; Song et al., 2008), personality, socialization, cognition and emotions (Finn et al., 2015; Greicius et al., 2003; Liégeois et al., 2019). Furthermore, Liu et al. (2018) have shown that fluid intelligence is significantly correlated with the predicted score based on the strength of dynamic FC matrices, and the observed cognitive flexibility and executive inhibition are significantly correlated with the predicted scores based on the variability of dynamic FC matrices. Therefore, all of these studies suggest that FC matrices contain behaviorally meaningful information.

4.2.3. Dynamic FC matrices computed with SSTD window-sizes capture cognitively and behaviorally meaningful information—As shown by Figs. 2–4 and Tables 3 and 4, better classification performances and higher explained behavioral variances are achieved when using dynamic FC matrices computed with SSTD window-sizes as features in the classification and regression analysis separately, as compared to using dynamic FC matrices computed with conventional fixed window-sizes. The frequency information of a non-stationary fMRI signal remains unstable and, therefore, a fixed window-size that is optimal for one time segment may not be suitable for other time segments. SSTD window-sizes, in contrast, are data-driven and time-dependent, allowing these subtle variations of the temporal dynamics to be captured.

4.3. Technical perspectives

4.3.1. Improvements over previous methods—As we introduced above, SSTD window-sizes are based on the multi-scale time-dependent intrinsic correlation method that was first proposed by Chen et al. (2010), where multiple window-sizes were computed for a single time point. Specifically, at a single time point, one window-size was determined for each IMF and a 2D heat plot was generated to represent the multi-scale intrinsic correlations between two time series (Chen et al., 2010). This method captures the time-dependent frequency information in the original time series but is difficult to interpret for BOLD signals in terms of FCs.

In Cordes et al. (2018), our group proposed a weighted average to combine these multiple window-sizes at each time point in the sliding-window dynamic FC analysis. It has been observed that the Hilbert Transform produces unstable results at cutting time points, and therefore extreme and oscillated window-sizes were obtained for the starting and ending time points in Cordes et al. (2018), leading to an average window-sizes of 97.75s ± 41.36s (Cordes et al., 2018). In the current study, we first improved the method to compute SSTD window-sizes by creating longer time series to ensure the continuity of the starting and ending time points and to avoid unstable and extreme results. In addition, from the method perspective, the number of IMFs in Cordes et al. (2018) was a fixed and predefined parameter. In the current method, the number of IMFs is determined from the data itself, and therefore the entire process in computing SSTD window-sizes is data-driven without any predefined parameters. As a result, average SSTD window-sizes computed for both data in the current study is around 34s, which is closer to values reported in Zalesky and Breakspear (2015). Furthermore, from a validation perspective, the combined window-size in Cordes et al. (2018) was only validated for BOLD signals with a TR of 2.4s using the dynamic states routine following Allen et al. (2014), where the number of dynamic states was another tuning parameter which may affect the results (discussed in more detail in the next section). In the current study, we validate SSTD window-sizes using fMRI data with TR = 2.8 and 0.72s respectively, which demonstrates the optimum performance of SSTD window-sizes over fixed window-sizes in the sliding-window analysis for BOLD signals with both low and high sampling rates. Finally, the current study quantifies dynamic FC matrices using the standard deviation of each FC over all slided windows, which is computed without any tuning parameters and is a more direct measure to compare performances between different window-sizes, as compared to the dynamic states routine.

4.3.2. Methods to estimate instantaneous frequency—In computing SSTD window-sizes, we used EMD combined with the Hilbert transform to estimate the instantaneous frequency of BOLD signals, which is the Hilbert Huang Transform (Huang and Shen, 2014). Analytically, the instantaneous frequency of a time signal is defined as the derivative of the phase (Cohen, 1989). For a real signal, the most common method to compute its phase is to build a complex signal with the original signal as the real part and the Hilbert Transform of the original signal as the imaginary part (Zhao et al., 2004). However, this method works only for the signal with a narrow frequency range, which is not the case for multicomponent BOLD signals. The Hilbert Huang transform works for the BOLD signals by applying EMD to decompose the original signal into IMFs, where each IMF

represents a simple oscillatory mode within a limited frequency band that meets the pre-request of the analytical method. Instead of EMD, narrow-band pass filters could also be applied to decompose the original BOLD signals into multiple time-series with limited frequency bands that are suitable for the Hilbert transform.

4.3.3. Other signal decomposition methods—As we stated above, EMD decomposes original BOLD signals into multiple IMFs with different frequency components. Other methods also can be applied to represent BOLD signals in terms of multiple frequency components, such as the Fourier transform and the Wavelet transform (Chang and Glover, 2010). Both Fourier and Wavelet transforms require a predefined fixed basis function and give a bounded time-frequency relationship, which work well for time series with known underlying physical processes. However, underlying process of BOLD signals are usually difficult to define. On the other hand, EMD requires no a priori defined basis functions and uses data itself to determine the underlying frequency information. Therefore, in our study, we used EMD, instead of Fourier or wavelet transform, to decompose BOLD signals.

4.3.4. Using standard deviation to quantify temporal dynamics over all slided windows—Following computing windowed FC matrices, most studies perform a clustering analysis to identify different brain-states based on spatial similarities among all windowed FC matrices, and used the clustered brain-states to quantify temporal dynamics (Allen et al., 2014; Damaraju et al., 2014; Sakoğlu et al., 2010). We do not use the classified brain states, mainly because, in this method, the number of brain-states is another parameter to be pre-determined. Functional connections within each brain-state, time points spent in each brain-state and frequency of brain-state transitions significantly depend on this predefined number. Furthermore, in a classification framework with dynamic FC as input features similar to the framework used in our study, the number of features increases linearly with the pre-defined number of brain-states, which could easily exceed the number of subjects and thus make it difficult for classification framework to produce meaningful results. In addition, Choe et al. (2017) have demonstrated that the fluctuation of dynamic FC (i.e. its variance) has a strong potential to provide individual-specific differences. Finally, Liu et al. (2018) compute dynamic FC strength, stability, and variability to characterize temporal dynamics over all slided windows and show that these measurements could successfully identify individuals with high accuracy and reliably predict higher individual cognitive performance. In our study, similar ideas are applied, and the temporal dynamics of FC between an ROI pair is quantified by the standard deviation of this connection over all slided windows.

4.3.5. Using both static FC and dynamic FC matrices as dynamic FC features in classification and regression analysis—In our study, we always kept both static and dynamic FC matrices as dynamic features in both classification and regression analysis. Liu et al. (2018) defined the average of FC matrices over all slided windows as dynamic FC mean strength and considered it as one of the dynamic characteristic measurements. The same measurement was computed in our study for both *PFBHS* data and *HCP* data. High spatial similarities between the static FC matrix and dynamic FC mean strength matrix were observed for both data (Supplementary Fig. S3). Therefore, in our study, a static FC matrix

was used to represent the dynamic FC mean strength, and was used together with the standard deviation matrix as features for both classification and regression analysis.

4.3.6. Using two datasets to validate SSTD window-sizes—We used two fMRI data to validate SSTD window-sizes in this study, one with a conventional sampling rate (TR = 2.8s, *PFBHS* data) and a total duration of 6mins and 20s; and the other one with a faster sampling rate (TR = 0.72s, *HCP* data) and a total duration of 14mins and 20s. For fMRI data with a low sampling rate, temporal changes may be missed due to under-sampling of the fMRI signal, whereas for fMRI data with a high sampling rate, the captured temporal changes may be sensitive to spurious noises. Therefore, we have validated SSTD window-sizes in both cases in the current study. The larger explained behavioral variance and higher classification accuracy when using SSTD window-sizes suggest that SSTD window-sizes were able to capture temporal dynamics in fMRI data with both low and high sampling rates.

4.4. Limitations and future directions

One limitation of the SSTD window-sizes method is that the performance may deteriorate as the noise level in BOLD signals increases. The first step of the SSTD window-sizes method is to decompose BOLD signals into IMFs using the EMD method. Despite the capability of dealing with nonlinear and non-stationary data, EMD still cannot resolve the signal from the noise in complicated cases, especially when the noise has the same time scale as the signal (Wu and Huang, 2004). Future performance comparisons of the SSTD window-sizes method on BOLD signals with different de-noising strategies are needed to test and clarify the noise effects of the SSTD window-sizes method.

Furthermore, EMD is currently run on the entire concatenated time series; therefore, the number of IMFs is the same for all time points and remains static. For longer fMRI time series, the number of IMFs may also vary at different time points. One way to achieve a dynamic number of IMFs is to run EMD separately on each time series segment, which will increase the computational cost and is also less stable with shorter segments. After the EMD step, instantaneous period at every time point and average energy across all time points are used to compute the SSTD window-sizes in the current method. In this case, while the period is dynamically calculated at every time point, the energy is still assumed to be static across all time points. Static assumptions on both the energy and the number of IMFs may not be the most appropriate for a dynamic analysis. Future efforts towards computing an accurate time-dependent energy measure and determining dynamic number of IMFs at each time point, if possible, may further improve the performance of SSTD window-sizes. However, whether these extra dynamics reflect the intrinsic temporal variations of human brain function or just random noises also require further evaluations.

Another limitation of the current study is our use of simple sinusoidal signals with frequency shifts in our simulation to demonstrate that SSTD window-sizes capture the exact period (frequency) information at every time point (sections 2.2 and 3.1). Real fMRI signals are much more complicated than sinusoidal signals due to mixed frequency contents, physiological and electronic noise sources. We refrained from using more elaborate simulations with mixed frequency content because the ground-truth of the signal becomes

difficult, if not impossible, to define. Nevertheless, future efforts toward generating simulated signals that both have known frequency contents and represent signal distributions mimicking more real fMRI data may provide alternatives to validate SSTD window-sizes. In addition, previous studies have suggested that the variance of dynamic FC values derived from sliding-window approach with fixed window-sizes are less reliable than the dynamic conditional correlation derived measures (Choe et al., 2017). Future efforts towards the reproducibility analysis of sliding-window approach with SSTD window-sizes and the comparisons with other dynamic FC analysis methods are required to further validate our method.

5. Conclusion

Single-scale time-dependent window-sizes (SSTD) have been computed in the sliding-window method for dynamic FC analysis. SSTD window-sizes are based on the frequency contents of the time series and computed with EMD and a spectral analysis using the Hilbert Huang Transform. Simulation has demonstrated that SSTD window-sizes are data-driven, time-dependent and capture the exact frequency content in the time series. Using dynamic FC matrices computed with SSTD window-sizes as features, both a higher classification accuracy between cognitively impaired and nonimpaired fighters and a larger explained behavioral variance in normal healthy adults are achieved, as compared to using dynamic FC computed with multiple conventional fixed window-sizes as features. Both classification and regression results have demonstrated that SSTD window-sizes are able to capture cognitive-function-related and behaviorally meaningful temporal dynamics information in resting-state fMRI data. MATLAB codes used to compute SSTD window-sizes and generate the simulation in this manuscript are available on GitHub (https://github.com/EEHULULU/dynamicFC_optimum_windowsize.git).

Supplementary Material

Refer to Web version on PubMed Central for supplementary material.

Acknowledgement

The study is supported by the National Institutes of Health (grant 1R01EB014284 and P20GM109025), a private grant from the Peter and Angela Dal Pezzo funds, a private grant from Lynn and William Weidner, a private grant from Stacie and Chuck Matthewson, and the young scientist award at Cleveland Clinic Lou Ruvo Center for Brain Health (Keep Memory Alive Foundation). The *PFBHS* is supported by Belator, UFC, the August Rapone Family Foundation, Top Rank, and Haymon Boxing. *HCP* data were provided by the Human Connectome Project, WU-Minn Consortium (Principal Investigators: David Van Essen and Kamil Ugurbil; 1U54MH091657), which is funded by the 16 NIH Institutes and Centers that support the NIH Blueprint for Neuroscience Research; and by the McDonnell Center for Systems Neuroscience at Washington University.

References

Allen EA, Damaraju E, Plis SM, Erhardt EB, Eichele T, Calhoun VD, 2014 Tracking whole-brain connectivity dynamics in the resting state. Cerebr. Cortex 24, 663–676. 10.1093/cercor/bhs352.

Allen EA, Erhardt EB, Damaraju E, Gruner W, Segall JM, Silva RF, Havlicek M, Rachakonda S, Fries J, Kalyanam R, Michael AM, Caprihan A, Turner JA, Eichele T, Adelsheim S, Bryan AD, Bustillo J, Clark VP, Feldstein Ewing SW, Filbey F, Ford CC, Hutchison K, Jung RE, Kiehl KA, Kodituwakku P, Komesu YM, Mayer AR, Pearlson GD, Phillips JP, Sadek JR, Stevens M, Teuscher

U, Thoma RJ, Calhoun VD, 2011 A baseline for the multivariate comparison of resting-state networks. Front. Syst. Neurosci 5, 1–23. 10.3389/fnsys.2011.00002. [PubMed: 21347218]

Bai F, Watson DR, Yu H, Shi Y, Yuan Y, Zhang Z, 2009 Abnormal resting-state functional connectivity of posterior cingulate cortex in amnestic type mild cognitive impairment. Brain Res 1302, 167–174. 10.1016/j.brainres.2009.09.028. [PubMed: 19765560]

Baig S. ur R., Iqbal W, Berral JL, Carrera D, 2020 Adaptive sliding windows for improved estimation of data center resource utilization. Future Generat. Comput. Syst 104, 212–224. 10.1016/j.future.2019.10.026.

Behzadi Y, Restom K, Liau J, Liu TT, Behzadi Y, Restom K, Liau J, Liu TT, Restom Khaled, Liau Joy, Liu Thomas T., 2007 A component based noise correction method (CompCor) for BOLD and perfusion based fMRI. Neuroimage 37, 90–101. 10.1016/j.neuroimage.2007.04.042. [PubMed: 17560126]

Bernick C, Banks S, Phillips M, Lowe M, Shin W, Obuchowski N, Jones S, Modic M, 2013 Professional fighters brain health study: rationale and methods. Am. J. Epidemiol 178, 280–286. 10.1093/aje/kws456. [PubMed: 23735309]

Biswal B, Fz Y, Vm H, Js H, 1995 Functional connectivity in the motor cortex of resting human brain using echo-planar MRI. Magn. Reson. Med 34, 537–541. 10.1002/mrm.1910340409. [PubMed: 8524021]

Biswal BB, Mennes M, Zuo X-N, Gohel S, Kelly C, Smith SM, Beckmann CF, Adelstein JS, Buckner RL, Colcombe S, Dogonowski A-M, Ernst M, Fair D, Hampson M, Hoptman MJ, Hyde JS, Kiviniemi VJ, Kotter R, Li S-J, Lin C-P, Lowe MJ, Mackay C, Madden DJ, Madsen KH, Margulies DS, Mayberg HS, McMahon K, Monk CS, Mostofsky SH, Nagel BJ, Pekar JJ, Peltier SJ, Petersen SE, Riedl V, Rombouts SARB, Rypma B, Schlaggar BL, Schmidt S, Seidler RD, Siegle GJ, Sorg C, Teng G-J, Veijola J, Villringer A, Walter M, Wang L, Weng X-C, Whitfield-Gabrieli S, Williamson P, Windischberger C, Zang Y-F, Zhang H-Y, Castellanos FX, Milham MP, 2010 Toward discovery science of human brain function. Proc. Natl. Acad. Sci. Unit. States Am 107, 4734–4739. 10.1073/pnas.0911855107.

Calhoun VD, Adali T, Pearlson GD, Pekar JJ, 2001 Spatial and temporal independent component analysis of functional MRI data containing a pair of task-related waveforms. Hum. Brain Mapp 13, 43–53. 10.1002/hbm.1024. [PubMed: 11284046]

Calhoun VD, Miller R, Pearlson G, Adali T, 2014 The chronnectome: time-varying connectivity networks as the next frontier in fMRI data discovery. Neuron 84, 262–274. 10.1016/j.neuron.2014.10.015. [PubMed: 25374354]

Challis E, Hurley P, Serra L, Bozzali M, Oliver S, Cercignani M, 2015 NeuroImage Gaussian process classi fi cation of Alzheimer ' s disease and mild cognitive impairment from resting-state fMRI. Neuroimage 112, 232–243. 10.1016/j.neuroimage.2015.02.037. [PubMed: 25731993]

Chang C, Glover GH, 2010 Time-frequency dynamics of resting-state brain connectivity measured with fMRI. Neuroimage 50, 81–98. 10.1016/j.neuroimage.2009.12.011. [PubMed: 20006716]

Chen X, Wu Z, Huang NE, 2010 The time-dependent intrinsic correlation based on the empirical mode decomposition. Adv. Adapt. Data Anal 10.1142/S1793536910000471.

Chen X, Zhang H, Gao Y, Wee CY, Li G, Shen D, 2016 High-order resting-state functional connectivity network for MCI classification. Hum. Brain Mapp 37, 3282–3296. 10.1002/hbm.23240. [PubMed: 27144538]

Choe AS, Nebel MB, Barber AD, Cohen JR, Xu Y, Pekar JJ, Caffo B, Lindquist MA, 2017 Comparing test-retest reliability of dynamic functional connectivity methods. Neuroimage 158, 155–175. 10.1016/j.neuroimage.2017.07.005. [PubMed: 28687517]

Cohen L, 1989 Time-frequency distributions-A review. Proc. IEEE 77, 941–981. 10.1109/5.30749.

Cordes D, Zhuang X, Kaleem M, Sreenivasan K, Yang Z, Mishra V, Banks S, Bluett B, Cummings JL, 2018 Advances in functional magnetic resonance imaging data analysis methods using Empirical Mode Decomposition to investigate temporal changes in early Parkinson's disease. Alzheimer's Dement. Transl. Res. Clin. Interv 4, 372–386. 10.1016/J.TRCI.2018.04.009.

Damaraju E, Allen EA, Belger A, Ford JM, McEwen S, Mathalon DH, Mueller BA, Pearlson GD, Potkin SG, Preda A, Turner JA, Vaidya JG, Van Erp TG, Calhoun VD, 2014 Dynamic functional

connectivity analysis reveals transient states of dysconnectivity in schizophrenia. NeuroImage Clin 5, 298–308. 10.1016/j.nicl.2014.07.003. [PubMed: 25161896]

Damoiseaux JS, Rombouts SARB, Barkhof F, Scheltens P, Stam CJ, Smith SM, Beckmann CF, 2006 Consistent resting-state networks across healthy subjects. Proc. Natl. Acad. Sci. Unit. States Am 103, 13848–13853. 10.1073/pnas.0601417103.

De Luca M, Beckmann CF, De Stefano N, Matthews PM, Smith SM, 2005 fMRI resting state networks define distinct modes of long-distance interactions in the human brain Oxford Centre for Functional Magnetic Resonance Imaging of the Brain, UK. Neuroimage 10.1016/j.neuroimage.2005.08.035.

Desikan RS, Ségonne F, Fischl B, Quinn BT, Dickerson BC, Blacker D, Buckner RL, Dale AM, Maguire RP, Hyman BT, Albert MS, Killiany RJ, Se F, Fischl B, Quinn BT, Dickerson BC, Blacker D, Buckner RL, Dale AM, Maguire RP, Hyman BT, Albert MS, Killiany RJ, 2006 An automated labeling system for subdividing the human cerebral cortex on MRI scans into gyral based regions of interest. Neuroimage 31, 968–980. 10.1016/j.neuroimage.2006.01.021. [PubMed: 16530430]

Deypir M, Sadreddini MH, Hashemi S, 2012 Towards a variable size sliding window model for frequent itemset mining over data streams. Comput. Ind. Eng 63, 161–172. 10.1016/j.cie.2012.02.008.

Draper NR, Smith H, 1998 Applied Regression Analysis John Wiley & Sons.

Eavani H, Satterthwaite TD, Gur RE, Gur RC, Davatzikos C, 2013 Unsupervised learning of functional network dynamics in resting state fMRI. Inf. Process Med. Imaging 23, 426–437. 10.1007/978-3-642-38868-2_36. [PubMed: 24683988]

Finn ES, Shen X, Scheinost D, Rosenberg MD, Huang J, Chun MM, Papademetris X, Constable RT, 2015 Functional connectome fingerprinting: identifying individuals using patterns of brain connectivity. Nat. Neurosci 18, 1664–1671. 10.1038/nn.4135. [PubMed: 26457551]

Fischl B, 2012 FreeSurfer. Neuroimage 62, 774–781. 10.1016/j.neuroimage.2012.01.021. [PubMed: 22248573]

Fox MD, Snyder AZ, Vincent JL, Corbetta M, Van Essen DC, Raichle ME, 2005 From the Cover: the human brain is intrinsically organized into dynamic, anticorrelated functional networks. Proc. Natl. Acad. Sci. Unit. States Am 102, 9673–9678. 10.1073/pnas.0504136102.

Glasser MF, Sotiropoulos SN, Wilson JA, Coalson TS, Fischl B, Andersson JL, Xu J, Jbabdi S, Webster M, Polimeni JR, Van Essen DC, Jenkinson M, Consortium W-MH, 2013 The minimal preprocessing pipelines for the human connectome Project. Neuroimage 80, 105–124. 10.1021/nl061786n.Core-Shell. [PubMed: 23668970]

Gonzalez-Castillo J, Hoy CW, Handwerker DA, Robinson ME, Buchanan LC, Saad ZS, Bandettini PA, 2015 Tracking ongoing cognition in individuals using brief, whole-brain functional connectivity patterns. Proc. Natl. Acad. Sci. Unit. States Am 112, 8762–8767. 10.1073/pnas.1501242112.

Greicius M, 2008 Resting-state functional connectivity in neuropsychiatric disorders. Curr. Opin. Neurol 24, 424–430. 10.1097/WCO.0b013e328306f2c5.

Greicius MD, Krasnow B, Reiss AL, Menon V, 2003 Functional connectivity in the resting brain: a network analysis of the default mode hypothesis. Proc. Natl. Acad. Sci. U. S. A 100, 253–258. 10.1073/pnas.0135058100. [PubMed: 12506194]

Greicius MD, Srivastava G, Reiss AL, Menon V, 2004 Default-mode network activity distinguishes Alzheimer's disease from healthy aging: evidence from functional MRI. Proc. Natl. Acad. Sci. U. S. A 101, 4637–4642. 10.1073/pnas.0308627101. [PubMed: 15070770]

Gualtieri CT, Johnson LG, 2006 Reliability and validity of a computerized neurocognitive test battery, CNS Vital Signs. Arch. Clin. Neuropsychol 21, 623–643. 10.1016/j.acn.2006.05.007. [PubMed: 17014981]

Hindriks R, Adhikari MH, Murayama Y, Ganzetti M, Mantini D, Logothetis NK, Deco G, 2016 Can sliding-window correlations reveal dynamic functional connectivity in resting-state fMRI? Neuroimage 127, 242–256. 10.1016/j.neuroimage.2015.11.055. [PubMed: 26631813]

Holtzheimer PE, Mayberg HS, 2011 Stuck in a rut: rethinking depression and its treatment. Trends Neurosci 34, 1–9. 10.1016/j.tins.2010.10.004. [PubMed: 21067824]

Huang NE, 2005 Introduction to the Hilbert Huang transform. Transform 5, 1–26. 10.1142/9789812703347_0001.

Huang NE, Shen SSP, 2014 Hilbert-huang Transform and its Applications, Control, Interdisciplinary Mathematical Sciences. WORLD SCIENTIFIC 10.1142/9789812703347.

Huang NE, Shen Z, Long SR, Wu MC, Shih HH, Zheng Q, Yen N-C, Tung CC, Liu HH, 1998 The empirical mode decomposition and the Hilbert spectrum for nonlinear and non-stationary time series analysis. Proc. R. Soc. A Math. Phys. Eng. Sci 454, 903–995. 10.1098/rspa.1998.0193.

Huang NE, Wu Z, 2008 A review on hilbert-huang Transform : method and its applications. Rev. Geophys 46, 1–23. 10.1029/2007RG000228.1.INTRODUCTION.

Huang Y, Schmitt FG, 2014 Time dependent intrinsic correlation analysis of temperature and dissolved oxygen time series using empirical mode decomposition. J. Mar. Syst 130, 90–100. 10.1016/j.jmarsys.2013.06.007.

Hutchison RM, Womelsdorf T, Allen EA, Bandettini PA, Calhoun VD, Corbetta M, Della Penna S, Duyn JH, Glover GH, Gonzalez-Castillo J, Handwerker DA, Keilholz S, Kiviniemi V, Leopold DA, de Pasquale F, Sporns O, Walter M, Chang C, 2013 Dynamic functional connectivity: promise, issues, and interpretations. Neuroimage 80, 360–378. 10.1016/j.neuroimage.2013.05.079. [PubMed: 23707587]

Jack CR, Knopman DS, Jagust WJ, Petersen RC, Weiner MW, Aisen PS, Shaw LM, Vemuri P, Wiste HJ, Weigand SD, Lesnick TG, Pankratz VS, Donohue MC, Trojanowski JQ, 2013 Tracking pathophysiological processes in Alzheimer's disease: an updated hypothetical model of dynamic biomarkers. Lancet Neurol 12, 207–216. 10.1016/S1474-4422(12)70291-0. [PubMed: 23332364]

Jones DT, Vemuri P, Murphy MC, Gunter JL, Senjem ML, Machulda MM, Przybelski SA, Gregg BE, Kantarci K, Knopman DS, Boeve BF, Petersen RC, Jack CR, 2012 Non-stationarity in the "resting brain's" modular architecture. PloS One 7, e39731 10.1371/journal.pone.0039731. [PubMed: 22761880]

Khazaee A, Ebrahimzadeh A, Babajani-Feremi A, 2017 Classification of patients with MCI and AD from healthy controls using directed graph measures of resting-state fMRI. Behav. Brain Res 322, 339–350. 10.1016/j.bbr.2016.06.043. [PubMed: 27345822]

Kiviniemi V, Vire T, Remes J, Elseoud AA, Starck T, Tervonen O, Nikkinen J, 2011 A sliding time-window ICA reveals spatial variability of the default mode network in time. Brain Connect 1, 339–347. 10.1089/brain.2011.0036. [PubMed: 22432423]

Leonardi N, Van De Ville D, 2015 On spurious and real fluctuations of dynamic functional connectivity during rest. Neuroimage 104, 430–436. 10.1016/j.neuroimage.2014.09.007. [PubMed: 25234118]

Li H, Wang L, 2017 A variable size sliding window based frequent itemsets mining algorithm in data stream. AIP Conf. Proc 1839 10.1063/1.4982511.

Liégeois R, Li J, Kong R, Orban C, Van De Ville D, Ge T, Sabuncu MR, Yeo BTT, 2019 Resting brain dynamics at different timescales capture distinct aspects of human behavior. Nat. Commun 10 10.1038/s41467-019-10317-7.

Lindquist MA, Xu Y, Nebel MB, Caffo BS, 2014 Evaluating dynamic bivariate correlations in resting-state fMRI: a comparison study and a new approach. Neuroimage 101, 531–546. 10.1016/j.neuroimage.2014.06.052. [PubMed: 24993894]

Liu J, Liao X, Xia M, He Y, 2018 Chronnectome fingerprinting: identifying individuals and predicting higher cognitive functions using dynamic brain connectivity patterns. Hum. Brain Mapp 39, 902–915. 10.1002/hbm.23890. [PubMed: 29143409]

Liu X, Duyn JH, 2013 Time-varying functional network information extracted from brief instances of spontaneous brain activity. Proc. Natl. Acad. Sci. Unit. States Am 110, 4392–4397. 10.1073/pnas.1216856110.

Majeed W, Magnuson M, Hasenkamp W, Schwarb H, Schumacher Eric H., Barsalou L, Keilholz SD, Schumacher EH, Barsalou L, Keilholz SD, 2011 Spatiotemporal dynamics of low frequency BOLD fluctuations in rats and humans. Neuroimage 54, 1140–1150. 10.1016/j.neuroimage.2010.08.030. Spatiotemporal. [PubMed: 20728554]

Mishra VR, Zhuang X, Sreenivasan KR, Banks SJSJ, Yang Z, Bernick C, Cordes D, 2017 Multimodal MR imaging signatures of cognitive impairment in active professional fighters. Radiology 10.1148/radiol.2017162403, 0, Ryan, J. O., Pakhomov, S. V. S., Marino, S., Berni.

Patrick F, Goncalves P, 2004 Empirical mode decomposition as data-drive wavelet-like expansions. Int. J. Wavelets, Multiresolut. Inf. Process 2, 1–20. 10.1142/s0129183107011200.

Preti MG, Bolton TAW, Van De Ville D, 2017 The dynamic functional connectome: state-of-the-art and perspectives. Neuroimage 160, 41–54. 10.1016/j.neuroimage.2016.12.061. [PubMed: 28034766]

Price T, Wee C-Y, Gao W, Shen D, 2014 Multiple-network classification of childhood autism using functional connectivity dynamics. In: International Conference on Medical Image Computing and Computer-Assisted Intervention, pp. 177–184. 10.1007/978-3-319-10443-0_23.

Rashid B, Arbabshirani MR, Damaraju E, Cetin MS, Miller R, Pearlson GD, Calhoun VD, 2016 Classification of schizophrenia and bipolar patients using static and dynamic resting-state fMRI brain connectivity. Neuroimage 134, 645–657. 10.1016/j.neuroimage.2016.04.051. [PubMed: 27118088]

Sakoğlu Ü, Pearlson GD, Kiehl KA, Wang YM, Andrew M, Calhoun VD, 2010 A method for evaluating dynamic functional network connectivity and task-modulation: application to schizophrenia. Magn. Reson. Mater. Phys. Biol. Med 23, 351–366. 10.1007/s10334-010-0197-8.A.

Shen H, Wang L, Liu Y, Hu D, 2010 Discriminative analysis of resting-state functional connectivity patterns of schizophrenia using low dimensional embedding of fMRI. Neuroimage 49, 3110–3121. 10.1016/j.neuroimage.2009.11.011. [PubMed: 19931396]

Smith SM, Fox PTM, Miller KL, Glahn DC, Fox PTM, Mackay CE, Filippini N, Watkins KE, Toro R, Laird AR, Beckmann CF, 2009 Correspondence of the brain's functional architecture during activation and rest. Proc. Natl. Acad. Sci. Unit. States Am 106, 13040–13045. 10.1073/pnas.0905267106.

Smith SM, Miller KL, Moeller S, Xu J, Auerbach EJ, Woolrich MW, Beckmann CF, Jenkinson M, Andersson J, Glasser MF, Van Essen DC, Feinberg DA, Yacoub ES, Ugurbil K, 2012 Temporally-independent functional modes of spontaneous brain activity. Proc. Natl. Acad. Sci. Unit. States Am 109, 3131–3136. 10.1073/pnas.1121329109.

Song M, Zhou Y, Li J, Liu Y, Tian L, Yu C, Jiang T, 2008 Brain spontaneous functional connectivity and intelligence. Neuroimage 41, 1168–1176. 10.1016/j.neuroimage.2008.02.036. [PubMed: 18434203]

Thompson GJ, Pan W-JJ, Magnuson ME, Jaeger D, Keilholz SD, 2014 Quasi-periodic patterns (QPP): large-scale dynamics in resting state fMRI that correlate with local infraslow electrical activity. Neuroimage 84, 1018–1031. 10.1016/j.neuroimage.2013.09.029. [PubMed: 24071524]

Tzourio-Mazoyer N, Landeau B, Papathanassiou D, Crivello F, Etard O, Delcroix N, Mazoyer B, Joliot M, 2002 Automated anatomical labeling of activations in SPM using a macroscopic anatomical parcellation of the MNI MRI single-subject brain. Neuroimage 15, 273–289. 10.1006/nimg.2001.0978. [PubMed: 11771995]

Van Essen DC, Smith SM, Barch DM, Behrens TEJ, Yacoub E, Ugurbil K, 2013 The Wu-Minn human connectome Project: an overview. Neuroimage 80, 62–79. 10.1016/j.neuroimage.2013.05.041. [PubMed: 23684880]

Wang ZHE, Zheng YU, Zhu DC, Bozoki AC, Li T, 2018 Classification of Alzheimer's disease, mild cognitive impairment and normal control subjects using resting-state fmri based network connectivity analysis. IEEE J. Transl. Eng. Heal. Med 6, 1–9. 10.1109/JTEHM.2018.2874887.

Wu - Minn Consortium Human Connectome Project, 2017 Wu-minn HCP 1200 Subjects Data Release: Reference Manual 2017, pp. 1–169. http://www.humanconnectome.org/documentation/S900/.

Wu Z, Huang NE, 2004 A study of the characteristics of white noise using the empirical mode decomposition method. Proc. R. Soc. A Math. Phys. Eng. Sci 460, 1597–1611. 10.1098/rspa.2003.1221.

Yaesoubi M, Miller RL, Bustillo J, Lim KO, Vaidya J, Calhoun VD, 2017 A joint time-frequency analysis of resting-state functional connectivity reveals novel patterns of connectivity shared

between or unique to schizophrenia patients and healthy controls. NeuroImage Clin 15, 761–768. 10.1016/j.nicl.2017.06.023. [PubMed: 28706851]

Yang Z, Zhuang X, Sreenivasan K, Mishra V, Curran T, Cordes D, 2019 A Robust Deep Neural Network for Denoising Task-Based fMRI Data: an Application to Working Memory and Episodic Memory 10.1101/746313 bioRxiv 746313.

Yu Q, Erhardt EB, Sui J, Du Y, He H, Hjelm D, Cetin MS, Rachakonda S, Miller RL, Pearlson G, Calhoun VD, 2015 Assessing dynamic brain graphs of time-varying connectivity in fMRI data: application to healthy controls and patients with schizophrenia. Neuroimage 107, 345–355. 10.1016/j.neuroimage.2014.12.020. [PubMed: 25514514]

Zalesky A, Breakspear M, 2015 Towards a statistical test for functional connectivity dynamics. Neuroimage 114, 466–470. 10.1016/j.neuroimage.2015.03.047. [PubMed: 25818688]

Zalesky A, Fornito A, Cocchi L, Gollo LL, Breakspear M, 2014 Time-resolved resting-state brain networks. Proc. Natl. Acad. Sci. Unit. States Am 111, 10341–10346. 10.1073/pnas.1400181111.

Zhang C, Dougherty CC, Baum SA, White T, Michael AM, 2018 Functional connectivity predicts gender: evidence for gender differences in resting brain connectivity. Hum. Brain Mapp 39, 1765–1776. 10.1002/hbm.23950. [PubMed: 29322586]

Zhao Z, Pan M, Chen Y, 2004 Instantaneous frequency estimate for non-stationary signal. In: Proceedings of the 5 World Congress on Intelligent Control and Automation, pp. 3641–3643.

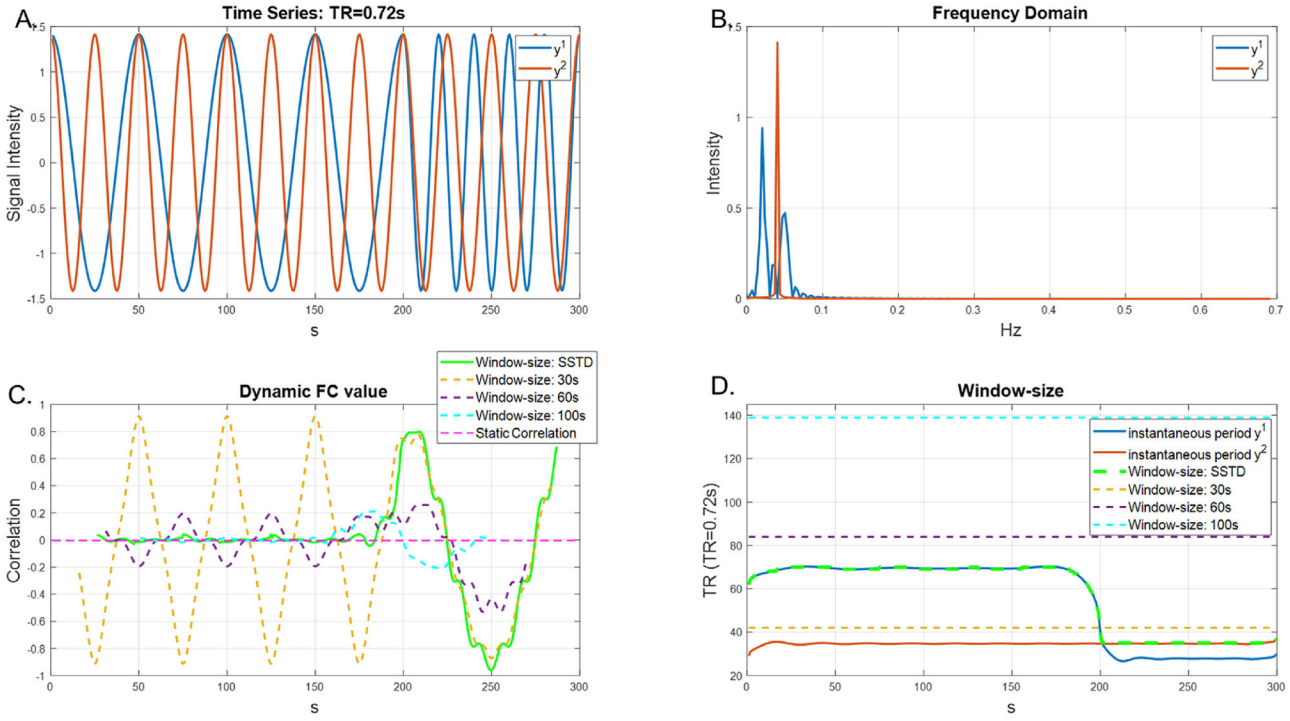

Fig. 1.

Simulation results of TR = 0.72s. (A). Simulated time series $y^{(1)}$ (blue) and $y^{(2)}$ (red). (B). Corresponding frequency spectrums. (C). Static FC values between two time series (dashed pink line). Dynamic FC values computed using the sliding-window method with SSTD window-sizes (solid green line) and multiple fixed window-sizes (dashed yellow, purple and light blue lines). (D). Instantaneous periods of $y^{(1)}$ (solid blue line) and $y^{(2)}$ (solid red line), SSTD window-sizes (dashed green line), and multiple fixed window-sizes (dashed yellow, purple and light blue lines).

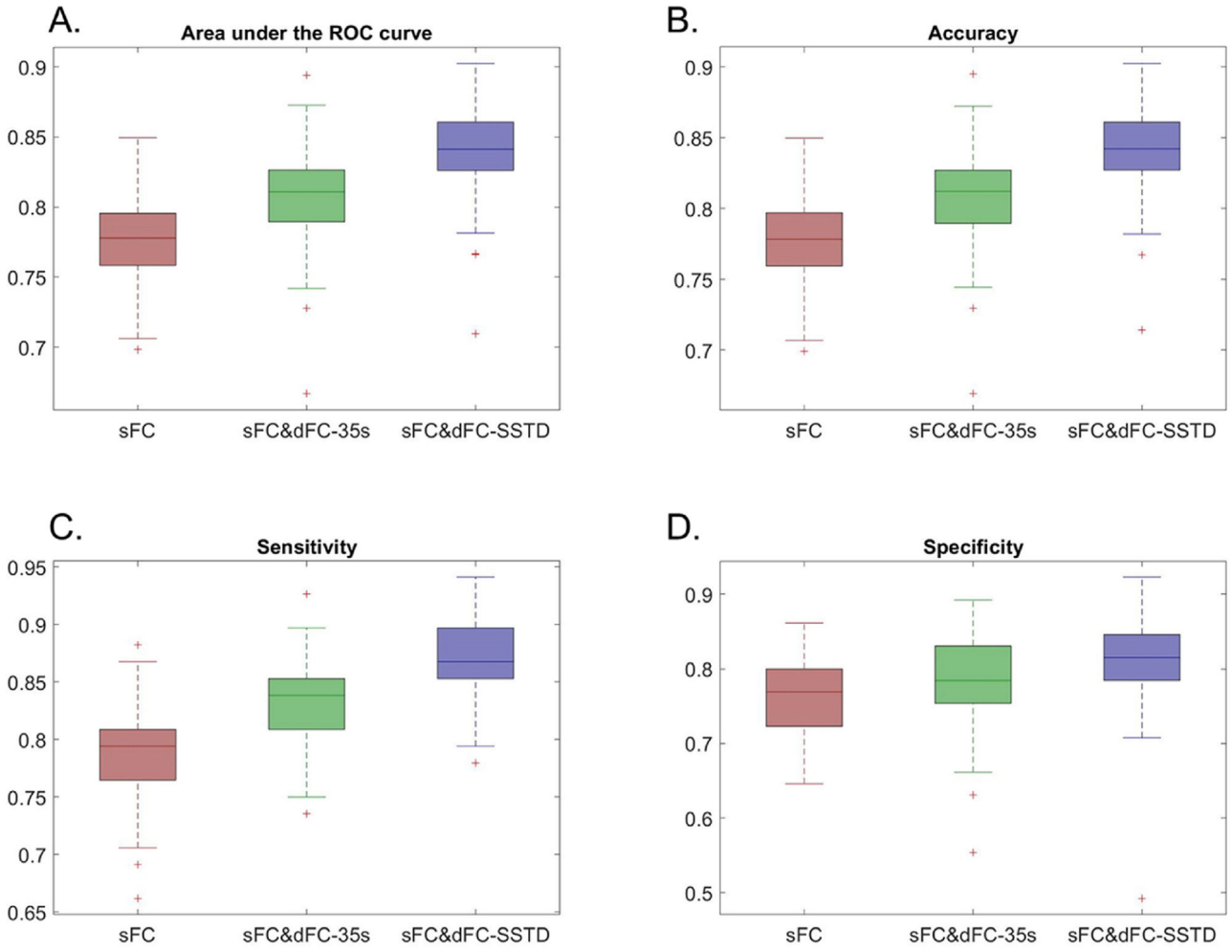

Fig. 2.

Classification results of the *PFBHS* data. Area under the ROC curve (A), accuracy (B), sensitivity (C) and specificity (D) of classification between cognitively nonimpaired and impaired fighters, when using static FC alone as features (red), using both static FC and dynamic FC computed with fixed window-size (35s) as features (green), and using both static FC and dynamic FC computed from SSTD window-sizes as features (purple). Boxplots show measurements of 100 iterations. Abbreviations: sFC: static functional connectivity; dFC-fixed-35s: dynamic functional connectivity matrix computed with the 35s window-size; dFC-SSTD: dynamic functional connectivity matrix computed with single-scale time-dependent window-sizes.

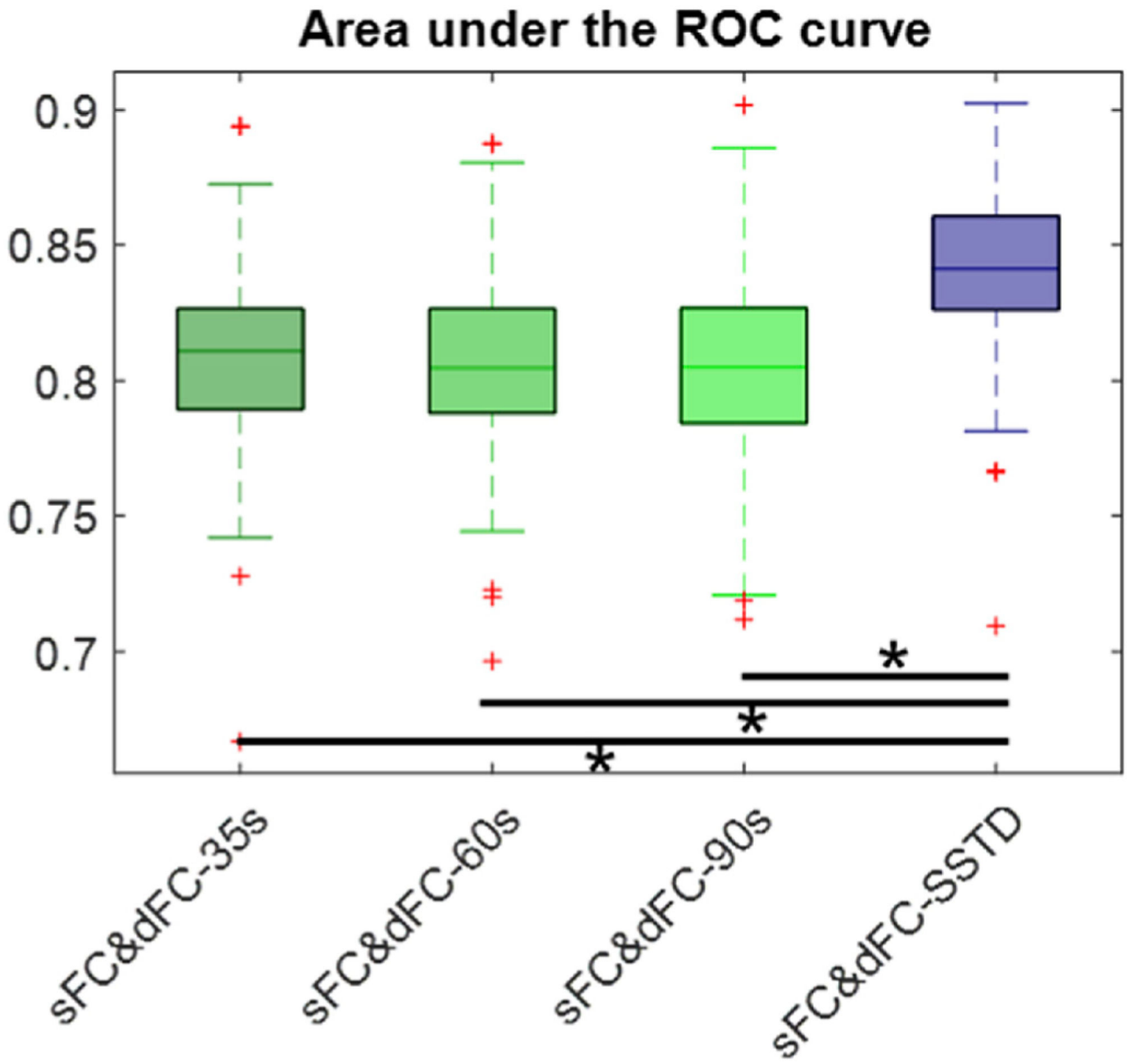

Fig. 3.

Classification results of the *PFBHS* data. Areas under the ROC curves of classification between cognitively nonimpaired and impaired fighters, when using both static FC and dynamic FC computed with SSTD window-sizes as features (purple box) and using both static FC and dynamic FC computed with multiple fixed window-sizes (green boxes). Boxplots show measurements of 100 iterations. * indicates statistically significant differences. Abbreviations: sFC: static functional connectivity matrices; dFC-fixed-35/60/90s: dynamic functional connectivity matrix computed with the 35/60/90s window-size (~12/21/32 TR); dFC-SSTD: dynamic functional connectivity matrix computed with single-scale time-dependent window-sizes.

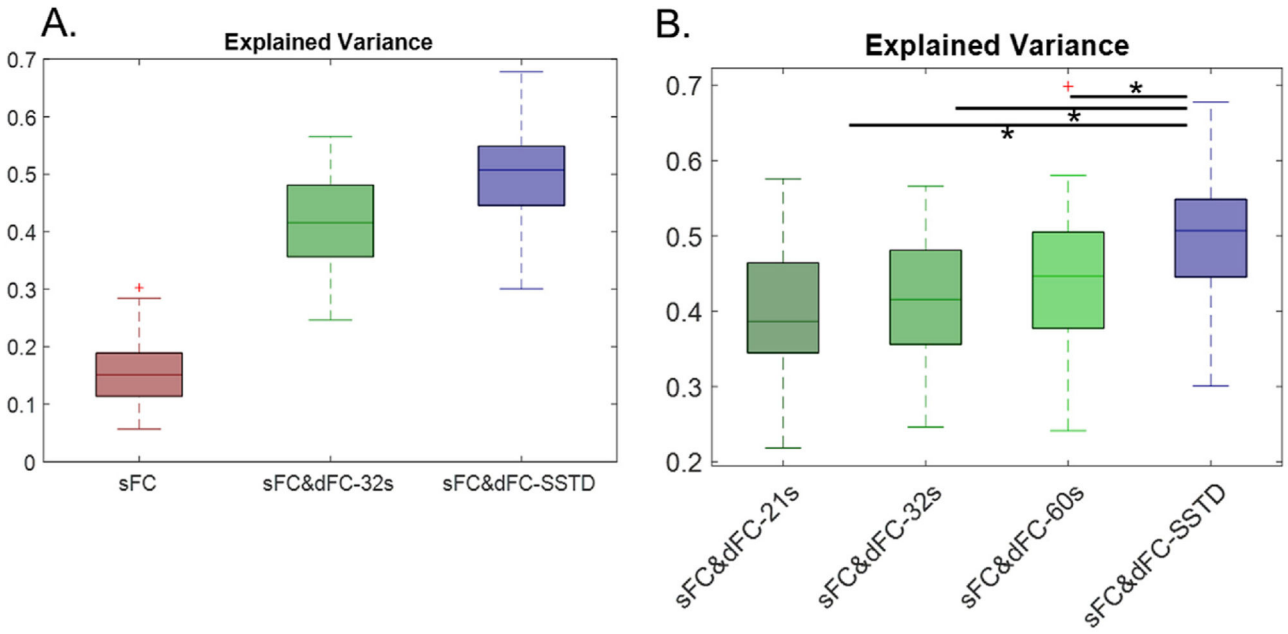

Fig. 4.

Regression analysis results of the *HCP* data. Boxplots of explained behavioral variance, when using static FC matrices as features alone (red box in A), both static and dynamic FC matrices computed with SSTD window-sizes as features (purple boxes in A and B), and both static and dynamic FC computed with multiple fixed window-sizes as features (green boxes in A and B). Abbreviations: sFC: static functional connectivity matrices; dFC-fixed-21/32/60s: dynamic functional connectivity matrix computed with the 21/32/60s window-size (~30/45/90 TR); dFC-SSTD: dynamic functional connectivity matrix computed with single-scale time-dependent window-sizes.

Table 1 (A)

Demographics of *PFBHS* subjects.

	Nonimpaired fighters	Impaired fighters	Group difference (p-value)
No. of Subjects	65	68	NA
Gender	58 Men	65 Men	0.16
	7 Women	3 Women	
Age at Imaging (years)	28.78 ± 5.27	29.78 ± 6.20	0.32
Years of Education (years)	13.28 ± 1.63	13.03 ± 2.12	0.45
Processing Speed score	58.28 ± 7.30	40.85 ± 8.34	<0.001
Psychomotor Speed score	183.12 ± 15.95	153.16 ± 16.11	<0.001
Number of Fights	14.45 ± 12.97	14.47 ± 12.68	0.99
Years of Fighting	6.03 ± 4.02	6.85 ± 4.45	0.27
Knock-outs	0.78 ± 1.14	1.07 ± 1.83	0.27
fMRI motion (mm)	0.23 ± 0.09	0.25 ± 0.11	0.30

Table 1 (B)

Demographics of *HCP* subjects.

	Normal Subject
No. of Subjects	88
Gender	88 Men
Age at Imaging (years)	27.71 ± 1.28
Years of Education (years)	15.03 ± 1.65
fMRI motion	Passed *HCP* quality control

Table 2

Repetition time (TR) and average SSTD window-sizes computed for both *HCP* data and *PFBHS* data.

	***HCP* data**	***PFBHS* data**	
		Nonimpaired fighters	**Impaired fighters**
TR (s)	0.72	2.8	
Duration	14mins and 24s	6mins and 24s	
Average SSTD window- sizes (s)	32.73 ± 3.52	34.66 ± 2.29	34.20 ± 2.29

Table 3

Classification results of the *PFBHS* data: statistical significances (p-values) of different dynamic FC matrices as features in the classification analysis. Abbreviations: sFC: static functional connectivity matrices; dFC-fixed-35/60/90s: dynamic functional connectivity matrix computed with the 35/60/90s window-size (~12/21/32 TR); dFC-SSTD: dynamic functional connectivity matrix computed with single-scale time-dependent window-sizes.

	sFC&dFC-35s	**sFC&dFC-60s**	**sFC&dFC-90s**	**sFC&dFC-SSTD**
sFC&dFC-35s	NA	0.55	0.43	1.52E-10
sFC&dFC-60s	0.55	NA	0.86	1.33E-11
sFC&dFC-90s	0.43	0.86	NA	3.04E-12
sFC&dFC-SSTD	1.52E-10	1.33E-11	3.04E-12	NA

Table 4

Regression results of the *HCP* data: statistical significances (p-values) of explained behavioral variances when using different dynamic FC matrices as features. Abbreviations: sFC: static functional connectivity matrices; dFC-fixed-21/32/60s: dynamic functional connectivity matrix computed with the 21/32/60s window-size (~30/45/90 TR); dFC-SSTD: dynamic functional connectivity matrix computed with single-scale time-dependent window-sizes.

	sFC&dFC-21s	**sFC&dFC-32s**	**sFC&dFC-60s**	**sFC&dFC-SSTD**
sFC&dFC-21s	NA	0.39	0.01	1.18E-08
sFC&dFC-32s	0.39	NA	0.10	4.93E-07
sFC&dFC-60s	0.01	0.10	NA	5.15E-04
sFC&dFC-SSTD	1.18E-08	4.93E-07	5.15E-04	NA